Research Square

Preprints are preliminary reports that have not undergone peer review.
They should not be considered conclusive, used to inform clinical practice,
or referenced by the media as validated information.

Homology modelling and molecular dynamics evaluation of kaempferol and quercetin binding to litchi polyphenol oxidase

Sakshi Sinha
Indian Institute of Technology Kharagpur
Rishikesh Ratan
rishikeshratan169@gmail.com

Indian Institute of Technology Kharagpur

Research Article

Keywords: polyphenol oxidase, homology modelling, molecular docking, postharvest, kaempferol, quercetin

Posted Date: September 17th, 2026

DOI: https://doi.org/10.21203/rs.3.rs-10867514/v1

License: This work is licensed under a Creative Commons Attribution 4.0 International License.
Read Full License

Additional Declarations: No competing interests reported.

Homology modelling and molecular dynamics evaluation of kaempferol and quercetin binding to litchi polyphenol oxidase

Sakshi Sinha[1], Rishikesh Ratan*[2]

[1]Rajendra Mishra School of Engineering Entrepreneurship, Indian Institute of Technology Kharagpur, West Bengal 721302, India

[2]Agricultural and Food Engineering Department, Indian Institute of Technology Kharagpur, West Bengal, 721302, India

***Corresponding author:** rishikeshratan169@gmail.com

Abstract

Postharvest pericarp browning, caused principally by the enzymatic oxidation of endogenous phenolics by polyphenol oxidase (PPO), is a major factor limiting the shelf life and commercial value of litchi (*Litchi chinensis* Sonn.), yet no experimental three-dimensional structure of litchi PPO (LcPPO) is available and its candidate inhibitors have not previously been examined at the molecular level. This work establishes a structure-based, dynamics-tested framework for evaluating candidate anti-browning agents against LcPPO. A validated homology model of the mature enzyme, with its binuclear type-3 copper centre reconstituted and its auto-inhibitory C-terminal domain removed, was used to screen fourteen compounds. The two best-ranked litchi flavonols, kaempferol (−6.89 kcal/mol) and quercetin (−6.58 kcal/mol), obtained more favourable scores than the natural substrate (−)-epicatechin and were predicted to occupy the substrate-access channel, with quercetin forming more hydrogen bonds than kaempferol. Independent 20 ns molecular dynamics simulations showed that, although the enzyme remained structurally stable, neither flavonol persistently maintained its docked pose: quercetin reoriented abruptly at approximately 4–5 ns and kaempferol migrated more gradually, behaviour corroborated by RMSD, hydrogen-bond and centre-of-mass analyses, though both ligands remained protein-associated throughout. Classical metal-chelating inhibitors scored weakly, reflecting the inability of empirical docking to represent copper coordination; as both docking and simulation used a copper-free receptor, the two mechanistic classes are not directly comparable and copper-chelation mechanisms were not assessed. ADMET analysis indicated favourable predicted physicochemical and absorption properties, with no major toxicity alerts. These findings identify kaempferol and quercetin as candidates for experimental evaluation and indicate that shallow-channel binding

alone may be insufficient for durable engagement, providing a structural foundation for the design of natural anti-browning agents.

Keywords: polyphenol oxidase; homology modelling; molecular docking; postharvest; kaempferol; quercetin

1. Introduction

Litchi (*Litchi chinensis Sonn.*), a subtropical member of the Sapindaceae, is among the most commercially valuable fruits of Asia and is increasingly traded worldwide for its translucent, sweet-acidic aril and its rich content of polyphenols, anthocyanins, vitamin C and other bioactive constituents (Castillo-Olvera et al. 2025; Nacif et al. 2001). The commercial appeal of the fruit, however, rests heavily on the bright red colour of its pericarp, and this is precisely where the crop is most vulnerable: within one to two days of harvest at ambient temperature, the pericarp browns rapidly, losing its characteristic redness and acquiring a dull brown appearance that consumers reject. Because this deterioration is visible, fast and irreversible, pericarp browning is universally regarded as the single most important factor limiting the postharvest shelf life, marketability and export potential of litchi, and it is responsible for substantial economic losses across the supply chain each season (Bhushan et al. 2015; Liang et al. 2026).

At the biochemical level, litchi pericarp browning arises from two coupled processes: the degradation of the red anthocyanin pigments and the enzymatic oxidation of phenolic compounds. The latter is driven chiefly by polyphenol oxidase (PPO), with a contributing role from peroxidase (Deshi et al. 2022; Jiang et al. 2004). PPO is a type-3 copper metalloenzyme whose active site contains a binuclear pair of copper ions, each coordinated by three conserved histidine residues; it catalyses the oxidation of o-diphenols to highly reactive o-quinones, which then polymerise non-enzymatically and react with anthocyanins and proteins to form brown, melanin-like pigments (Pollard 2018). In litchi, PPO is compartmentalised away from its phenolic substrates in the intact fruit, but harvest-induced membrane damage, water loss and pigment breakdown bring enzyme and substrate together, triggering the browning cascade (Wang et al. 2026). The litchi PPO gene (LcPPO) has been cloned and characterised; its expression correlates closely with pericarp PPO activity and the browning index across cultivars and storage regimes, and recent gene-editing work has established (−)-epicatechin as its primary natural substrate, providing a clear biochemical reference point for the catalytic pocket (Wang et al. 2025).

Considerable effort has therefore been directed at controlling litchi PPO activity. Current postharvest practice relies on a combination of low-temperature storage, controlled- or modified-atmosphere packaging, and chemical dips such as sulfur dioxide fumigation and treatments with organic acids (citric, oxalic, ascorbic), glutathione, cysteine and hexylresorcinol (Bhushan et al. 2015; Huang et al. 2024; Sivakumar et al. 2010). While partially effective, these approaches face several limitations: sulfur dioxide leaves residues and raises food-safety and regulatory concerns, cold storage is costly and logistically demanding, and many chemical treatments provide only short-lived protection or alter fruit flavour (Kumar et al. 2026). There is thus a growing demand for safe, natural, food-compatible anti-browning agents — ideally ones that act directly on PPO. However, the molecular interactions between candidate inhibitors and litchi PPO have not yet been characterised at a structural level, and inhibitor selection has consequently remained largely empirical rather than mechanism-guided.

Computer-aided approaches such as molecular docking and molecular dynamics (MD) simulation offer a means to address this limitation by predicting how candidate molecules bind the enzyme and prioritising them before laboratory testing, thereby reducing experimental cost and effort (Hu et al. 2026). Their application to litchi PPO, however, has been constrained by two specific challenges that are addressed in the present study. First, no experimental three-dimensional structure of litchi PPO is available, so the receptor itself must be constructed and validated before docking can be undertaken. Second, plant PPOs are synthesised in a latent form in which a C-terminal domain physically shields the active site, and the catalytic centre depends on two copper ions that standard modelling and docking tools do not reproduce automatically; both features must be handled explicitly for the model to be biologically meaningful. A further, more general consideration is methodological: docking provides only a static, single-pose estimate, and a favourable docking score does not necessarily correspond to a stable complex, so such predictions require validation through molecular dynamics.

The present study addresses these challenges in an integrated manner. A homology model of litchi PPO was constructed, its binuclear copper centre was reconstituted, the shielding domain was removed to generate the mature enzyme, and the model was validated by re-docking the natural substrate. Using this validated receptor, a panel of litchi-derived polyphenols and established food-grade inhibitors was screened, the binding modes of the leading candidates were characterised by both three- and two-dimensional interaction analysis, and the two best-ranked

flavonols were subjected to independent 20 ns MD simulations and a series of trajectory analyses to examine whether their predicted binding was maintained. Complementary ADMET profiling was performed to assess their predicted physicochemical and toxicity profiles. In doing so, the study provides the first structure-based, dynamics-tested assessment of anti-browning candidates against litchi PPO, and it yields a mechanistically informative finding, namely that high-scoring flavonol poses were not necessarily retained over the simulated trajectories, with implications for the rational design of natural browning inhibitors.

2. Materials and Methods

2.1 LcPPO sequence retrieval and homology modelling

The amino-acid sequence of litchi polyphenol oxidase (599 residues) was retrieved from the NCBI GenBank database (nucleotide accession JF926153; protein accession AEQ30073.1). The sequence comprises an N-terminal chloroplast transit peptide, a central catalytic type-3 copper domain, and a C-terminal shielding domain characteristic of latent plant polyphenol oxidases. A three-dimensional structural model was generated using the SWISS-MODEL server (Bordoli et al. 2009). The crystal structure of latent apple tyrosinase (MdPPO1; PDB ID: 6ELS; 1.3 Å resolution) was selected as the modelling template, as it represented the highest-quality copper-containing structure available and shared 70.34% sequence identity with the target. The resulting model encompassed residues 128–598, with the transit peptide excluded during template alignment, and exhibited good stereochemical quality, with a Global Model Quality Estimate (GMQE) of 0.71 and a QMEANDisCo global score of 0.78 ± 0.05.

2.2 Active-site reconstruction and mature-enzyme preparation

The SWISS-MODEL server transferred only a single copper ion to the model, whereas the functional PPO active site contains two copper ions. The binuclear centre was therefore reconstituted using UCSF ChimeraX (Di Trani et al. 2023). The apple template (6ELS), which retains both catalytic copper ions, was superposed onto the model using the *matchmaker* command, yielding a backbone RMSD of 0.183 Å over 449 atom pairs, and both template copper ions were subsequently transferred into the litchi active site. The reconstituted centre contained two copper ions coordinated by six histidine residues (His183, His213, His335, His339, His368 and His369), consistent with the canonical three-histidine-per-copper arrangement characteristic of type-3

copper enzymes. Plant polyphenol oxidases are synthesised in a latent form in which a C-terminal domain physically shields the active site, and this domain was found to occlude the copper pocket during preliminary docking. Residues 456–598 were therefore deleted to generate the mature, catalytically accessible enzyme; all six copper-coordinating histidines reside below residue 370 and were consequently unaffected by the truncation. Hydrogen atoms were added at physiological protonation using the ChimeraX *addh* command. As the docking engine does not parameterise copper, the two copper ions were removed prior to receptor preparation, and docking was performed within the apo active-site pocket defined by the intact histidine cage. The resulting structure was converted to PDBQT format using the Meeko receptor-preparation script to yield a rigid receptor (Burendei et al. 2025).

2.3 Ligand preparation, molecular docking and validation

A screening panel of fourteen compounds was assembled for evaluation against the LcPPO active site. The panel comprised litchi-derived polyphenols (kaempferol, quercetin, gallic acid, ferulic acid, resveratrol, arbutin and catechol), established food-grade PPO inhibitors and reducing agents (kojic acid, ascorbic acid, citric acid, glutathione and 4-hexylresorcinol), the copper-chelating reference inhibitor tropolone, and melatonin. The natural substrate, (−)-epicatechin, was included as a validation control. Three-dimensional structures of all compounds were retrieved from the PubChem database and converted to PDBQT format using the Meeko ligand-preparation script, which assigns partial charges, atom types and rotatable bonds (Bolton et al. 2011). The docking search space was centred on the midpoint of the two copper ions (x = 16.93, y = 39.65, z = 72.09 Å) and defined as a cubic grid box of 22 × 22 × 22 Å, encompassing the entire active-site cleft. Molecular docking was performed using AutoDock Vina (version 1.2.7) via its Python application programming interface, employing the Vina scoring function with an exhaustiveness value of 16 and generating up to ten poses per ligand (Tripathi et al. 2025). For each compound, the lowest-energy pose was retained as the representative binding affinity, and the complete panel was screened using a single automated Python script. The validity of the docking protocol was confirmed by re-docking the natural substrate, (−)-epicatechin, which bound within the copper pocket with an affinity of −6.39 kcal/mol and adopted a pose in which its catechol hydroxyl groups were oriented toward the binuclear centre, thereby reproducing the expected substrate geometry. Protein–ligand interactions were characterised by three complementary approaches, each applied

to the same top-ranked docked pose and the same mature (truncated) receptor: geometric contact and hydrogen-bond analysis in UCSF ChimeraX, two-dimensional interaction diagram generation using the PoseView tool implemented in the ProteinsPlus server, and hydrogen-bond identification with MDTraj at the start of the molecular dynamics trajectory (Ehrt et al. 2025; McGibbon et al. 2015; Noriega et al. 2025). These methods apply different distance and angular criteria for hydrogen-bond assignment and different radii for hydrophobic contact, and the molecular dynamics analysis is performed on the solvated, energy-minimised system rather than on the raw docked pose. The number of interactions reported by each method therefore differs, and the results obtained from each are reported separately rather than combined.

2.4 Molecular dynamics simulations

The dynamical stability of the two leading complexes, kaempferol–LcPPO and quercetin–LcPPO, was assessed by means of independent all-atom molecular dynamics simulations. For each complex, the top-ranked docked pose was exported with restored bond orders and combined with the mature protein, which had been protonated at pH 7.4 using PDBFixer. The simulations were performed on the apo (copper-free) complexes for two reasons: the catalytic copper ions cannot be represented by standard biomolecular force fields without bespoke parameterisation, and the flavonols bind the substrate-access channel rather than coordinating the metal centre. This simplification is therefore justified for the ligands considered here. The protein was described using the Amber FF14SB force field, and each ligand was parameterised with GAFF2 (gaff-2.11) using the OpenMM-Forcefields package, with ligand molecules handled via the OpenFF Toolkit (Rufa 2025). Each complex was solvated in a TIP3P water box with a padding of 1.0 nm and neutralised with 0.15 M NaCl, yielding a system of approximately 95,500 atoms. Long-range electrostatic interactions were treated using the particle-mesh Ewald method with a 1.0 nm cut-off, and all bonds to hydrogen atoms were constrained. Following energy minimisation and equilibration, a 20 ns production trajectory was generated for each complex using a Langevin-Middle integrator (300 K; 1 ps^{-1} collision frequency; 2 fs time step) under a Monte Carlo barostat maintained at 1 bar (Mohamed 2025). All simulations were executed on a graphics processing unit (GPU) using the OpenCL platform of OpenMM 8.5.2, with atomic coordinates saved every 10 ps.

2.5 Trajectory analysis

Trajectory analysis was carried out using MDTraj, with periodic images corrected by molecular imaging prior to all calculations. Conformational stability was quantified from the root-mean-square deviation (RMSD) of the protein backbone and of the ligand heavy atoms, computed relative to the energy-minimised starting structure. Local flexibility was evaluated from the per-residue root-mean-square fluctuation (RMSF) of the Cα atoms, and the overall compactness of the system was assessed from the radius of gyration (Rg) of the protein backbone and of the ligand (Alahdal et al. 2026). Retention of each ligand within the binding site was monitored through the protein–ligand centre-of-mass (COM) distance. Hydrogen-bond dynamics were characterised using two complementary approaches. First, the donor–acceptor distance of each candidate protein–ligand hydrogen bond identified in the docked pose, according to the Baker–Hubbard criteria, was tracked frame-by-frame throughout the trajectory (Duong 2020). These criteria were applied inclusively so as to enumerate all candidate interactions, including marginal geometries, since the purpose of the analysis was to determine which contacts persisted during the simulation. Second, the pooled distribution of these distances was expressed as an occupancy probability distribution. Finally, the collective backbone motions of each complex were examined by principal component analysis (PCA) of the Cα coordinates.

2.6 ADMET prediction and software

The pharmacokinetic, physicochemical and toxicity profiles of the two lead compounds were predicted from their canonical SMILES representations using two complementary web servers. The SwissADME server was employed to determine physicochemical properties, lipophilicity, water solubility and gastrointestinal absorption, together with drug-likeness parameters including Lipinski's rule of five, the bioavailability score, PAINS and Brenk structural alerts, and synthetic accessibility (Daina et al. 2017). The pkCSM server was used to predict absorption, distribution, metabolism and excretion properties, as well as key toxicity endpoints, namely AMES mutagenicity, hepatotoxicity, hERG I and II inhibition, and skin sensitisation (Gunasekaran et al. 2026).

The complete set of software employed in this study is summarised as follows: SWISS-MODEL for homology modelling; UCSF ChimeraX (version 1.12) for structure editing, copper reconstitution, hydrogen addition and analysis; Meeko (version 0.7.1) together with RDKit and Open Babel for receptor and ligand preparation; AutoDock Vina (version 1.2.7) for molecular

docking; PoseView, implemented in the ProteinsPlus server, for two-dimensional interaction diagrams; OpenMM (version 8.5.2), together with PDBFixer, the OpenFF Toolkit and OpenMM-Forcefields, for molecular dynamics system preparation and simulation; and MDTraj for trajectory analysis. Protein sequence and compound structure data were obtained from the NCBI GenBank and PubChem databases, respectively.

3. Results and Discussion

3.1 Model quality and active-site integrity

The LcPPO homology model was of good quality (GMQE 0.71; QMEANDisCo 0.78 ± 0.05), reflecting the high identity (70.34%) to the apple PPO template and the near-identical backbone superposition (RMSD 0.183 Å). The overall fold of the mature enzyme, with its active site located in a central cleft, is shown in Figure 1.

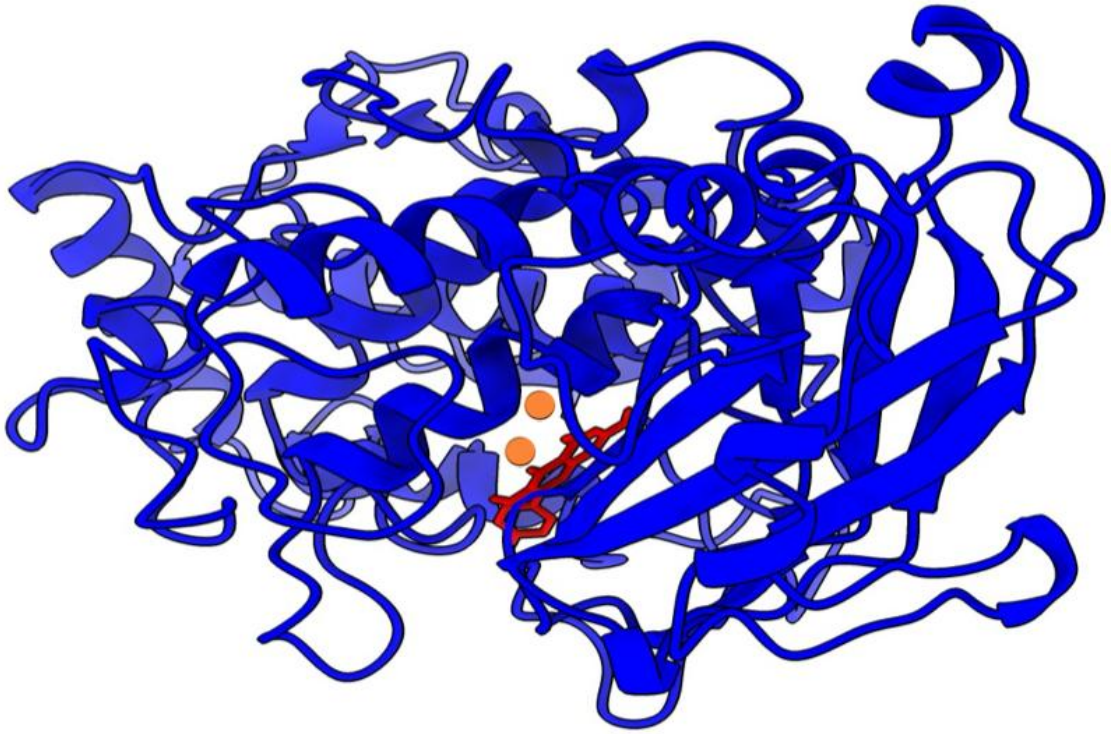


Figure 1. Three-dimensional homology model of mature litchi polyphenol oxidase (LcPPO). The protein is represented as a cartoon, coloured as a spectrum from the N-terminus (blue) to the C-terminus (red), with the two active-site copper ions shown as orange spheres. The model was constructed using the latent apple polyphenol oxidase structure (PDB ID: 6ELS; 70.34% sequence

identity) as a template and truncated to the mature, catalytically accessible form by removal of the C-terminal shielding domain.

Reconstitution of the binuclear copper centre produced an active site in which two copper ions were cradled by six histidine residues (Figure 2), matching the conserved architecture of plant type-3 copper enzymes and confirming that the catalytic geometry required for meaningful docking was preserved.

3.2 Validation with the natural substrate

Docking of (−)-epicatechin returned a top affinity of −6.39 kcal/mol, with the ten generated poses clustered narrowly between −5.8 and −6.4 kcal/mol. The best pose located the substrate within the active-site cleft, in contact with the copper-coordinating histidines His335 and His339 at the rim of the binuclear centre as well as with the surrounding channel residues (Figure 3), an orientation consistent with that expected for a catechol substrate poised for oxidation. The agreement between a favourable binding energy and a mechanistically plausible pose supports the validity of the receptor, grid box and scoring configuration, and provides a substrate baseline against which the candidate compounds could be assessed. As the copper ions were absent during docking, the pose reproduces the position of the substrate within the cleft but not the metal-coordinated geometry expected during catalysis.

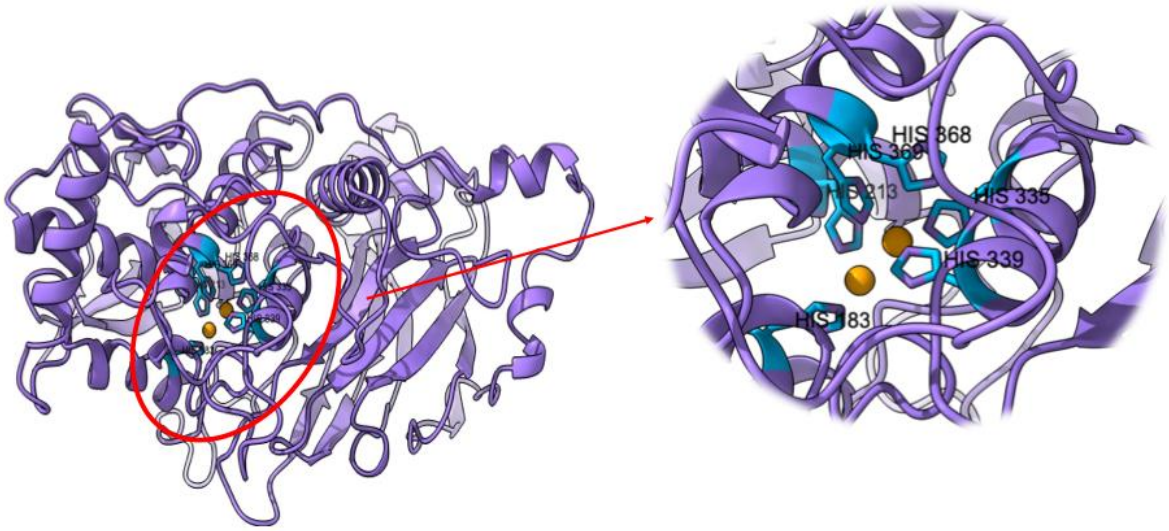


Figure 2. Reconstituted binuclear type-3 copper centre of LcPPO. The protein is represented as a purple cartoon, with the two catalytic copper ions shown as orange spheres coordinated by six

histidine residues (His183, His213, His335, His339, His368 and His369) displayed as sticks. The arrangement reproduces the canonical three-histidine-per-copper geometry characteristic of plant polyphenol oxidases.

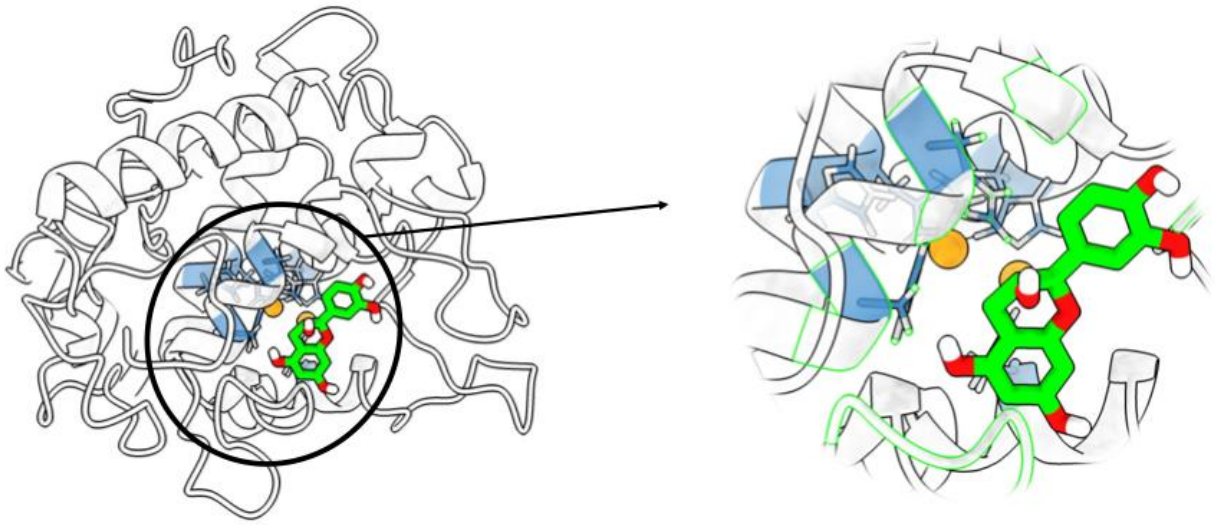


Figure 3. Validation of the docking protocol by re-docking of the natural substrate. The protein is shown as a pale grey semi-transparent cartoon, with (−)-epicatechin as green sticks, the two catalytic copper ions as orange spheres, and the copper-coordinating histidine residues as steel-blue sticks. In its top-ranked pose (−6.39 kcal/mol), the substrate occupies the active-site cleft in contact with His335 and His339 at the rim of the binuclear copper centre, an orientation consistent with that expected for a catechol substrate poised for oxidation.

3.3 Virtual screening of anti-browning candidates

The ranked docking results for the full panel, together with the substrate baseline, are presented in Table 1 and summarised graphically in Figure 4. Two litchi flavonols, kaempferol (−6.89 kcal/mol) and quercetin (−6.58 kcal/mol), bound the active site more strongly than the natural substrate, marking them as the leading candidate inhibitors. Arbutin, resveratrol and melatonin formed a second tier close to the substrate baseline; notably, melatonin — recently reported to delay litchi browning experimentally — scored favourably, providing independent structural support for that observation.

Table 1. Binding affinities of the screened compounds against the mature LcPPO active site, ranked from strongest to weakest. The natural substrate (−)-epicatechin (highlighted) serves as the validation baseline.

Rank	Compound	Binding affinity (kcal/mol)	Class / role
1	Kaempferol	−6.89	Flavonol (litchi polyphenol)
2	Quercetin	−6.58	Flavonol (litchi polyphenol)
3	**Epicatechin**	**−6.39**	**Natural substrate — baseline**
4	Arbutin	−6.29	Hydroquinone glycoside
5	Resveratrol	−6.15	Stilbenoid
6	Melatonin	−6.07	Indoleamine
7	4-Hexylresorcinol	−5.57	Resorcinol; food anti-browning agent
8	Ferulic acid	−5.41	Hydroxycinnamic acid
9	Glutathione	−4.89	Thiol tripeptide
10	Gallic acid	−4.81	Hydroxybenzoic acid
11	Tropolone	−4.69	Copper chelator (reference inhibitor)
12	Citric acid	−4.50	Chelating acid
13	Catechol	−4.35	Diphenol
14	Ascorbic acid	−4.06	Reducing agent
15	Kojic acid	−4.06	Copper chelator

A compound with a more favourable predicted binding affinity than the substrate could, in principle, occupy the active site and thereby impede epicatechin oxidation. On this basis, the litchi flavonols kaempferol and quercetin — bulky polyphenols bearing multiple hydroxyl groups capable of hydrogen bonding to the histidine cage — emerge as the most promising substrate-competitive anti-browning leads identified in this screen (Figure 4).

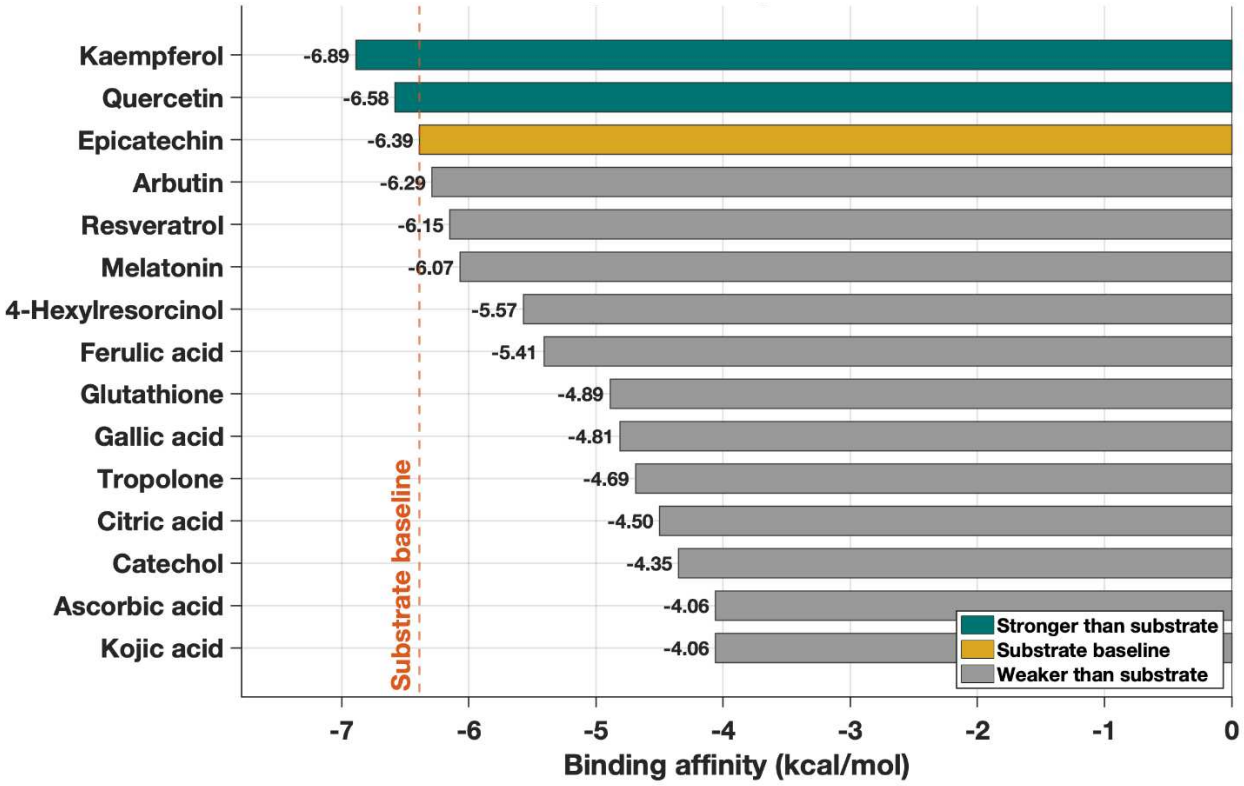


Figure 4. Binding affinities of the fourteen screened compounds against the mature LcPPO active site, ranked from strongest to weakest..

3.4 Binding modes of the lead compounds

The highest-ranked docking pose of kaempferol exhibited a binding energy of −6.89 kcal mol^{-1} and was positioned within the substrate-access channel near the entrance of the active site, rather than directly interacting with the binuclear copper centre (Figure 5). The ligand was stabilised by a hydrogen-bonding interaction at a distance of approximately 3.0 Å, together with several non-covalent contacts (<4.0 Å) involving eleven residues lining the active-site channel, namely Asn205, Ala327, Glu331, Asn332, Gly336, Pro337, Leu340, Gly354, Asn355, Phe356, and Tyr357. Among these residues, the aromatic side chains of Phe356 and Tyr357 were favourably positioned to support π–π interactions with the aromatic ring system of kaempferol, whereas the polar residues Asn205, Glu331, and Asn332 may contribute to ligand stabilisation through interactions with its hydroxyl groups. The remaining residues predominantly constitute the hydrophobic environment of the substrate-access channel and may further contribute to ligand accommodation within the binding pocket. Within this apo model, none of the six copper-

coordinating histidines lay within 4 Å of the ligand, indicating that the predicted pose occupies the substrate-access channel rather than the metal centre. If kaempferol does inhibit LcPPO, these results suggest a channel-occluding rather than a copper-chelating mode, though coordination in the holoenzyme cannot be excluded, as the simulations were performed without copper. Instead, its localisation within the substrate-entry region indicates a potential steric-blocking mechanism in which occupancy of the access channel may restrict substrate entry into the catalytic centre. Thus, the docking results support a putative substrate-competitive mode of inhibition, consistent with the favourable binding energy of kaempferol and its higher docking rank relative to the natural substrate.

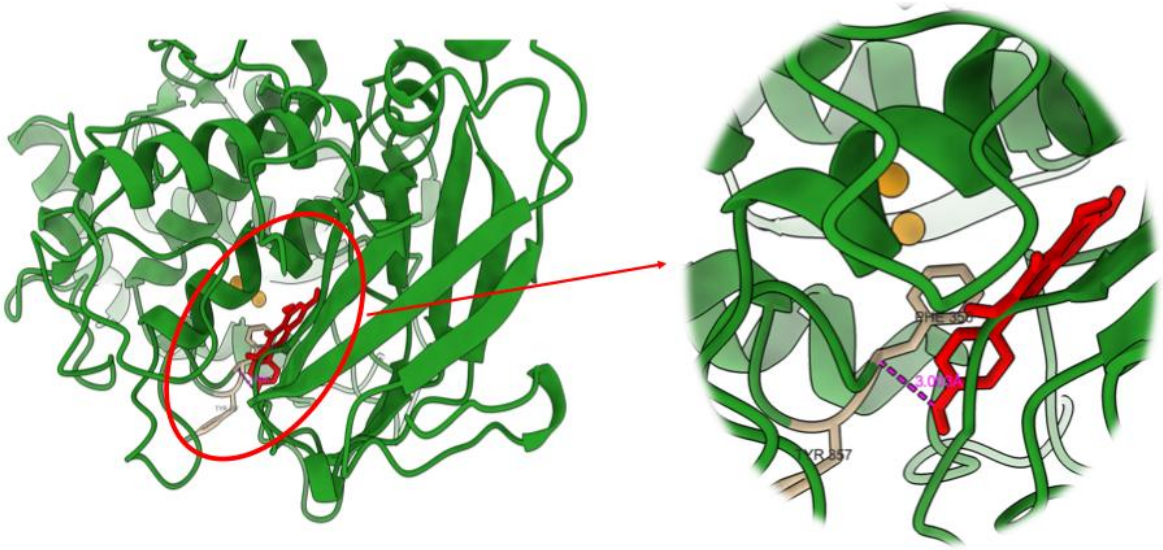


Figure 5. Predicted binding orientation of kaempferol within the active-site channel of LcPPO. The protein is represented as a green cartoon, kaempferol as wheat-coloured sticks, the two catalytic copper ions as orange spheres, and neighbouring active-site residues as green sticks. The cyan dashed line indicates a hydrogen-bonding interaction (~3.0 Å). Kaempferol is positioned within the substrate-access channel adjacent to the binuclear copper centre, where it is stabilised by hydrogen-bonding and aromatic interactions with Phe356 and Tyr357, without directly coordinating the catalytic copper ions.

Quercetin, which exhibited the second-highest docking affinity (−6.58 kcal mol^{-1}), adopted a binding orientation similar to that of kaempferol but was positioned deeper within the LcPPO active-site pocket (Figure 6). The ligand formed one hydrogen-bonding interaction with the

receptor and established close contacts (<4.0 Å) with eleven residues lining the active-site region. Nine of these residues—Glu331, Asn332, Gly336, Pro337, Leu340, Gly354, Asn355, Phe356, and Tyr357—were also involved in kaempferol binding, indicating substantial overlap in the interaction network of the two flavonols. In contrast to kaempferol, quercetin additionally interacted with His335 and His339, both of which participate in the coordination of the catalytic copper ions. This deeper positioning suggests that quercetin extends further toward the binuclear copper centre and engages residues located at the periphery of the catalytic metal-binding environment. Thus, quercetin appears to retain the substrate-channel occupancy observed for kaempferol while exhibiting additional proximity to the catalytic centre. Nevertheless, its slightly less favourable docking energy relative to kaempferol indicates that deeper penetration into the active-site pocket does not necessarily confer greater predicted binding affinity. Collectively, these findings suggest that kaempferol and quercetin may adopt closely related but distinct binding modes within the LcPPO active site, potentially interfering with substrate access and catalytic-site occupancy through complementary competitive interactions.

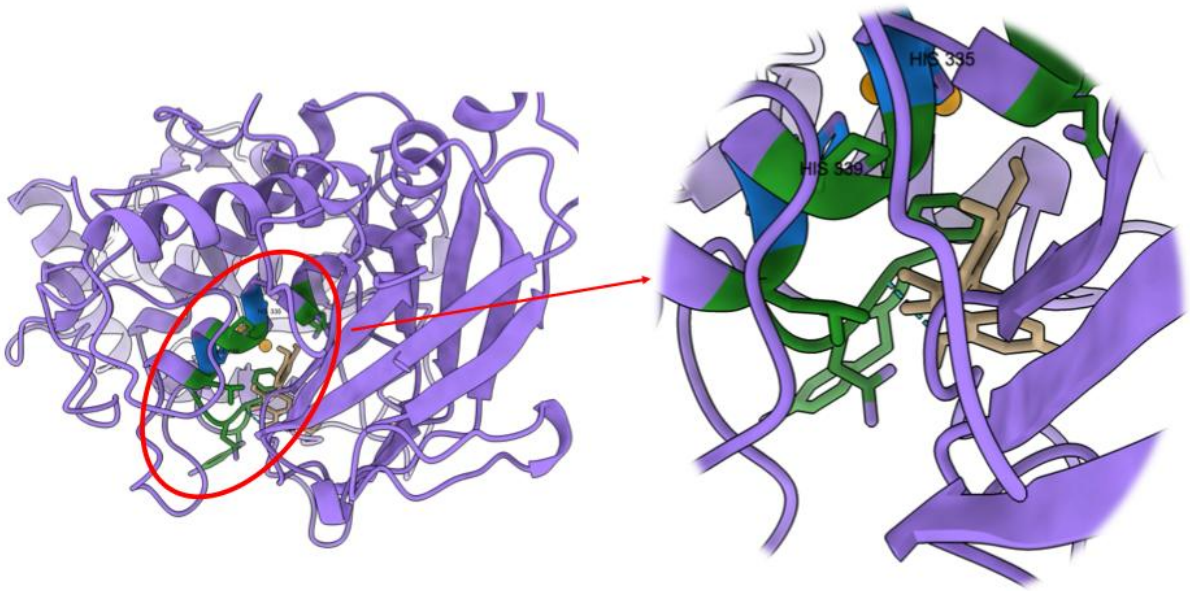


Figure 6. Predicted binding orientation of quercetin within the active-site pocket of LcPPO. The protein is represented as a purple cartoon, quercetin as wheat-coloured sticks, the two catalytic copper ions as orange spheres, and neighbouring active-site residues as green sticks. Quercetin occupies the substrate-access channel and extends deeper toward the binuclear copper centre than

kaempferol, establishing contacts with the copper-coordinating residues His335 and His339 in addition to interactions with residues lining the access channel.

The docked conformations of kaempferol and quercetin were further characterised using two-dimensional protein–ligand interaction diagrams generated with PoseView from the mature (truncated) receptor (Figure 7), enabling detailed identification of hydrogen-bonding, π-stacking and hydrophobic interactions within the LcPPO binding pocket. Kaempferol exhibited two hydrogen-bonding interactions, involving Asn205 and the backbone amide of Phe356, together with π-stacking and a hydrophobic contact involving Phe356. In comparison, quercetin displayed a more extensive hydrogen-bonding network, forming four hydrogen bonds with Phe356, Asn355, Glu331 and Asn332, alongside π-stacking and a hydrophobic contact with Phe356. The greater number of hydrogen-bonding interactions observed for quercetin may be attributed to its additional hydroxyl substituent, which provides a further site for polar interaction within the binding pocket. Phe356 emerged as the principal aromatic partner for both ligands, engaging each through a combination of backbone hydrogen bonding, π-stacking and hydrophobic contact. A comparative summary of the residues involved in the binding of both flavonols, classified according to interaction type, is presented in Table 2.

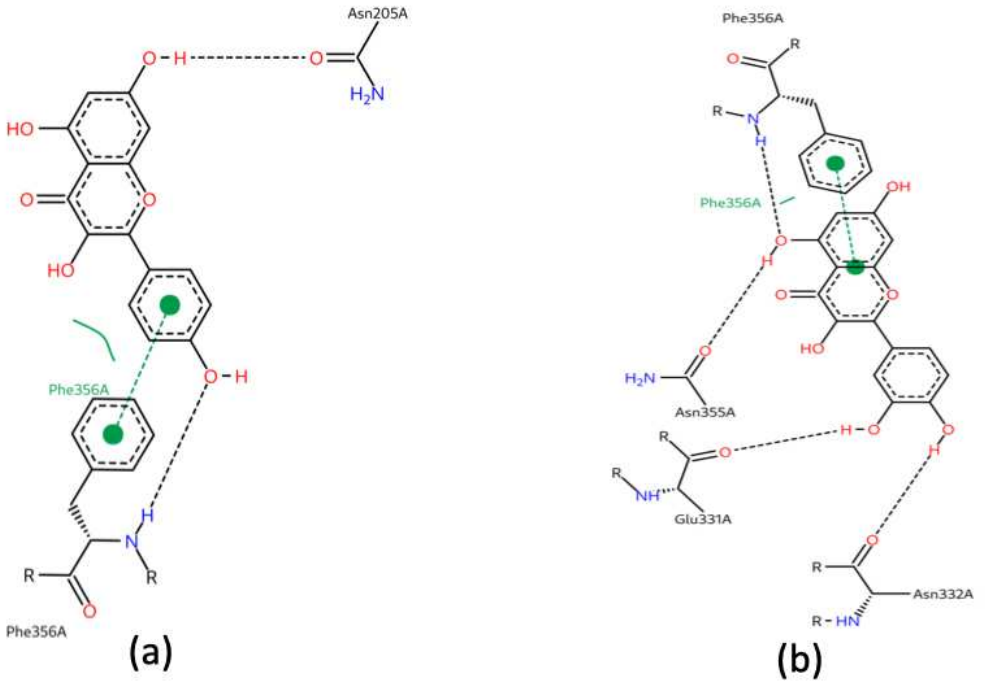


Figure 7. Two-dimensional protein–ligand interaction diagrams (PoseView) for the docked poses

of kaempferol (a) and quercetin (b) in the LcPPO active site. Dashed lines denote hydrogen bonds; green solid lines and filled circles denote π-stacking; green arcs denote hydrophobic contacts. Quercetin forms a greater number of hydrogen bonds, consistent with its additional hydroxyl group.

Table 2. Docking scores and interacting residues of the two lead flavonols with LcPPO. All interaction assignments were derived from the PoseView diagrams generated for the mature (truncated) receptor.

Compound	Docking score (kcal/mol)	H-bond (ChimeraX)	H-bond (PoseView)	π-Stacking	Contacts within 4 Å
Kaempferol	−6.89	Phe356 (2.0 Å)	Asn205, Phe356	Phe356	Asn205, Ala327, Glu331, Asn332, Gly336, Pro337, Leu340, Gly354, Asn355, Phe356, Tyr357
Quercetin	−6.58	Phe356 (1.8 Å)	Phe356, Asn355, Glu331, Asn332	Phe356	Glu331, Asn332, His335, Gly336, Pro337, His339, Leu340, Gly354, Asn355, Phe356, Tyr357

3.5 Molecular dynamics of the lead complex

To test whether the docked binding mode of the top lead is dynamically stable rather than a static artefact of rigid-receptor docking, the kaempferol–LcPPO complex was subjected to a 20 ns all-atom molecular dynamics simulation in explicit solvent. Throughout the trajectory the system remained well equilibrated, with the temperature maintained at 300 K and the potential energy stable. The LcPPO model was structurally sound: the protein backbone RMSD rose during initial relaxation, fluctuated around 4–7 Å in the middle of the run, and settled at approximately 2.6 Å over the final 5 ns, confirming that the homology model maintained its fold (Figure 8). The

backbone stabilises at ~2.6 Å, while the ligand tracks the protein for ~13 ns before diverging to ~11 Å, reflecting migration of kaempferol from the docked channel pose to an alternative surface site. The kaempferol ligand tracked the protein closely for the first ~13 ns (RMSD ~4–7 Å), indicating retention within the initial binding region, but thereafter diverged, its RMSD rising progressively to ~11 Å by the end of the simulation. Analysis of the final frame showed that the ligand remained in direct contact with the protein, the closest ligand–protein approach being 1.57 Å (a ligand hydroxyl hydrogen to the backbone carbonyl oxygen of Ala200), rather than dissociating into bulk solvent, indicating that kaempferol migrated from the docked channel-mouth pose to an alternative surface site. The docked pose is therefore best described as metastable: kaempferol occupies the shallow, solvent-exposed substrate-channel entrance transiently rather than being tightly anchored. This behaviour is consistent with the binding-mode analysis — in which kaempferol engaged the channel through a single hydrogen bond and hydrophobic contacts without reaching the buried copper centre — and it illustrates the value of molecular dynamics in distinguishing high-scoring but weakly retained poses from genuinely stable binding.

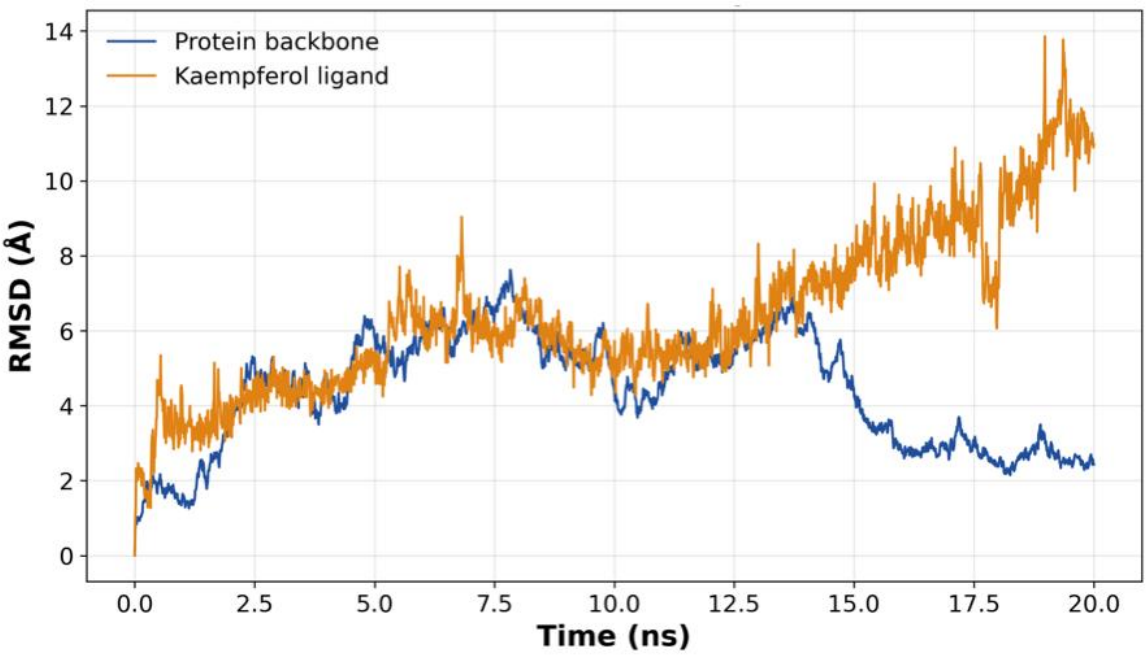


Figure 8. Root-mean-square deviation (RMSD) of the protein backbone and of the kaempferol ligand over the 20 ns molecular dynamics trajectory of the kaempferol–LcPPO complex, relative to the energy-minimised starting structure (periodic images corrected).

To establish whether this behaviour was specific to kaempferol or characteristic of the litchi flavonols at this site, an identical 20 ns simulation was performed for the second-ranked lead, quercetin, which had docked more deeply and contacted the copper-coordinating histidines His335 and His339. The outcome closely paralleled that obtained for kaempferol. The protein again remained structurally stable, with the backbone RMSD settling at approximately 2.7 Å, whereas the quercetin ligand RMSD increased from approximately 0.8 Å to 10.6 Å over the course of the trajectory (Figure 9). The ligand likewise remained in contact with the protein at the end of the simulation, the closest ligand–protein approach being 1.94 Å (a ligand hydroxyl hydrogen to the backbone carbonyl oxygen of Gly227), rather than dissociating into bulk solvent. Quercetin, despite its deeper initial pose, was therefore also not durably retained and migrated to an alternative surface site. The consistency of these two independent results is noteworthy. Both top-scoring litchi flavonols, although they registered favourable docking scores, failed to maintain their docked poses over 20 ns and behaved as transient, weakly anchored binders rather than as stably bound inhibitors. This convergent finding is consistent with the binding-mode analysis, in which each compound engaged its site through only a single hydrogen bond together with hydrophobic contacts. It further supports the central caveat of the present study, namely that shallow occupancy of the substrate channel is insufficient for durable inhibition, and that long-lived inhibition of litchi PPO is likely to require direct coordination of the catalytic copper centre, a chemistry captured neither by the flavonols themselves nor by the empirical docking scoring function. These observations also illustrate the value of the molecular dynamics step, since docking alone would have identified both flavonols as leads without revealing that their predicted poses are not sustained under realistic conditions.

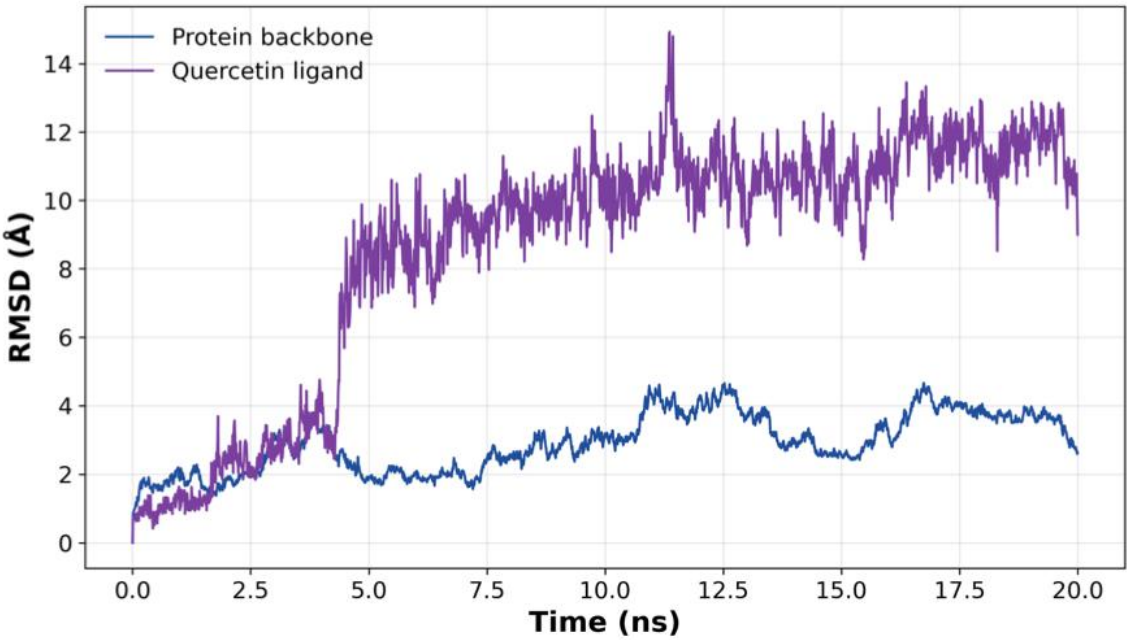


Figure 9. RMSD of the protein backbone (blue) and of the quercetin ligand (purple) over the 20 ns molecular dynamics trajectory of the quercetin–LcPPO complex (periodic images corrected). As for kaempferol, the backbone remains stable (~2.7 Å) while the ligand diverges to ~11 Å, indicating that quercetin also departs its docked pose despite binding more deeply in the initial docking.

3.6 Persistence of specific hydrogen bonds during dynamics

To determine precisely when and how the docked contacts were lost, every protein–ligand hydrogen bond present in the initial docked pose was identified and its donor–acceptor distance was tracked across the full 20 ns trajectory for both complexes (Figures 10 and 11).

For kaempferol, three candidate hydrogen bonds were present at the beginning of the simulation, formed with Glu331, Asn332 and Phe356. Of these, only the Glu331 contact was well formed (below 3.5 Å) at the outset, and it persisted for approximately the first 5–6 ns before breaking irreversibly. The Asn332 and Phe356 contacts remained marginal throughout the trajectory and never established a stable, sustained interaction. Kaempferol therefore lost its principal anchoring interaction within approximately the first quarter of the simulation, after which it continued to sample the channel and the adjacent surface in the absence of a dominant stabilising contact, consistent with the relocation subsequently identified by RMSD analysis.

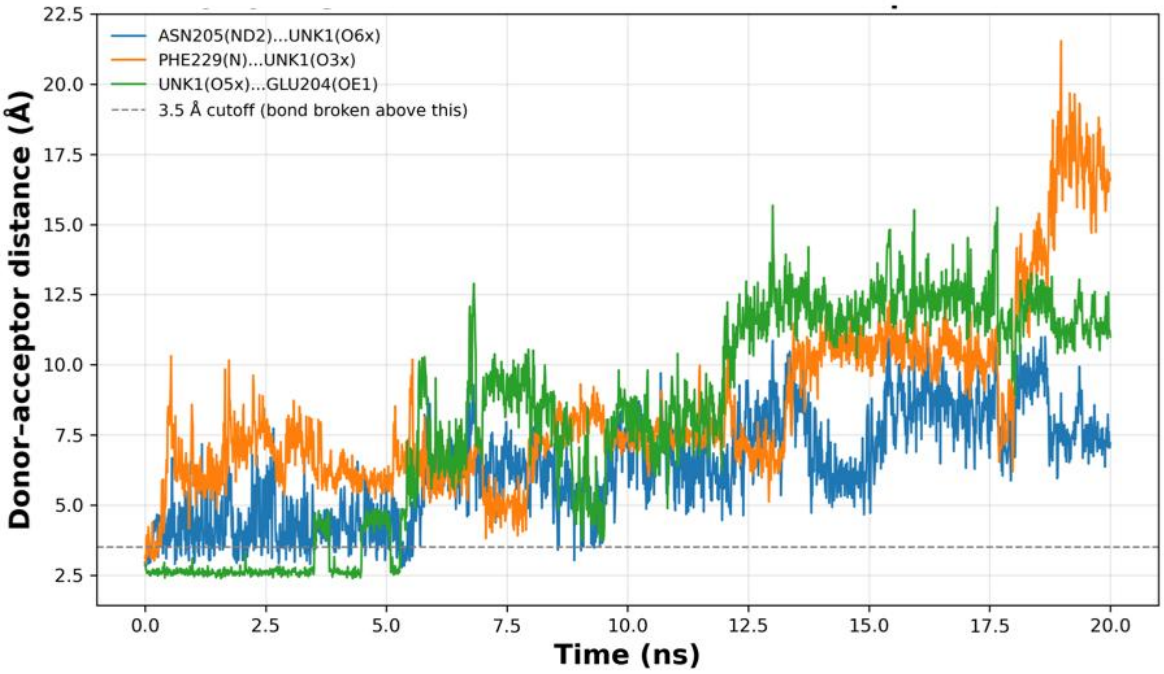


Figure 10. Donor–acceptor distance of the three candidate hydrogen bonds present in the docked kaempferol pose, tracked over the 20 ns trajectory. The Glu331 contact (green), the most persistent of the three, remains intact for approximately the first 5–6 ns before breaking irreversibly, whereas the Asn332 (blue) and Phe356 (orange) contacts are only marginally formed throughout.

Quercetin exhibited a markedly different and more informative pattern. Two of its six candidate hydrogen bonds, both formed with main-chain atoms (the amide N–H of Phe356 and the carbonyl oxygen of Gly354), remained at or below the 3.5 Å cut-off for almost the entire 20 ns trajectory and were essentially unbroken. In contrast, the four remaining contacts, all formed with polar or acidic side chains (Glu331, Asn205, Asp324 and Asp188), broke within approximately the first 4.5 ns and subsequently drifted to substantially larger distances of 10–25 Å for the remainder of the simulation. Two backbone contacts — Phe356(N) (blue) and Gly354(O) (orange) — remain intact for almost the entire simulation, while four side-chain contacts (green, red, purple, brown) break within the first ~4.5 ns and drift substantially, indicating that quercetin pivots on a persistent anchor rather than fully dissociating (Figure 11). This pattern indicates that quercetin does not fully dissociate from its original site, but rather pivots about a persistent two-point backbone anchor at the channel entrance, while its remaining hydroxyl substituents, no longer held by their original side-chain partners, become mobile and sample alternative, transient contacts. This behaviour reconciles the large overall ligand RMSD, which is dominated by the mobile distal

portion of the molecule, with the near-zero final-frame ligand–protein distance maintained by the persistent backbone anchor. Quercetin is therefore more accurately described as reorienting about a fixed point than as departing the site entirely.

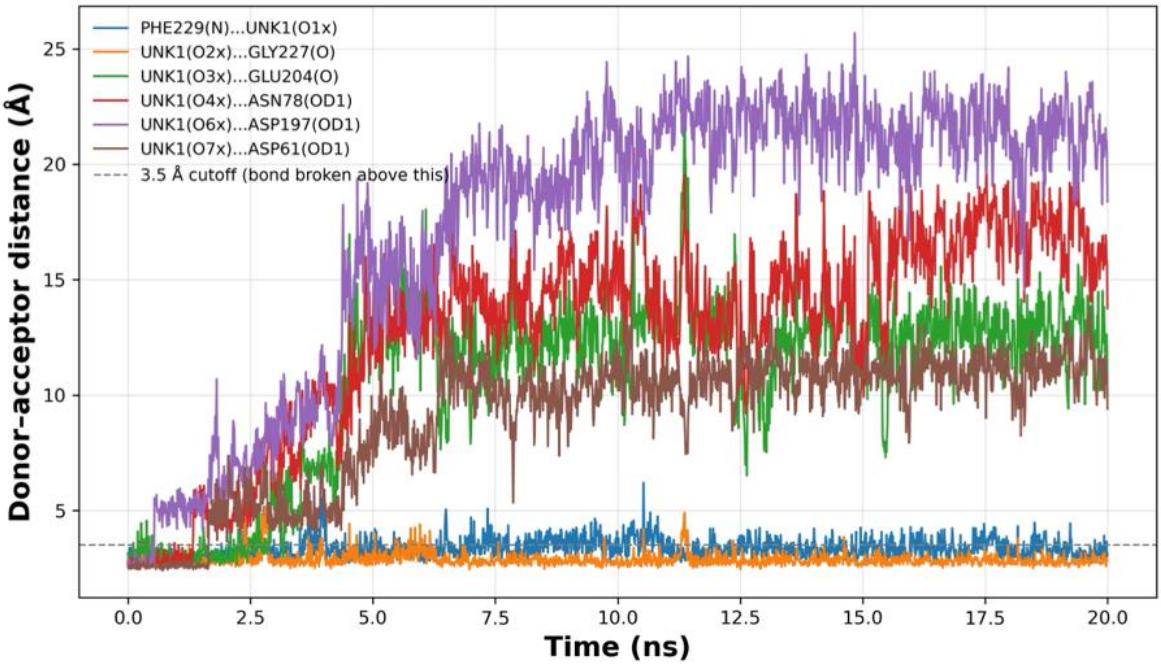


Figure 11. Donor–acceptor distance of the six candidate hydrogen bonds present in the docked quercetin pose, tracked over the 20 ns trajectory.

To complement the per-bond time series, the full population of candidate ligand hydrogen bonds was pooled across the trajectory and expressed as a probability distribution of donor–acceptor distance (Figure 12). For kaempferol, the pooled distribution was bimodal, comprising a sharp, well-defined peak at approximately 2.5–2.7 Å corresponding to genuine bonding, followed by a shallow trough and a rising tail extending toward 6 Å. This profile indicates that a substantial fraction of the trajectory involved fully broken contacts as the ligand drifted. For quercetin, the distribution was instead unimodal and right-skewed, dominated by a single strong peak at approximately 2.8–3.0 Å. As this distribution pools all six candidate bonds, its concentration near bonding distance reflects the statistical weight of the two persistent backbone-anchored contacts (Phe356 and Gly354), notwithstanding the loss of the four side-chain contacts. The occupancy analysis therefore corroborates the time-resolved picture. The hydrogen bonding of kaempferol is essentially binary, being either formed or broken, whereas the aggregate bonding of quercetin

remains statistically weighted toward short distances throughout the simulation, consistent with its persistent partial anchor.

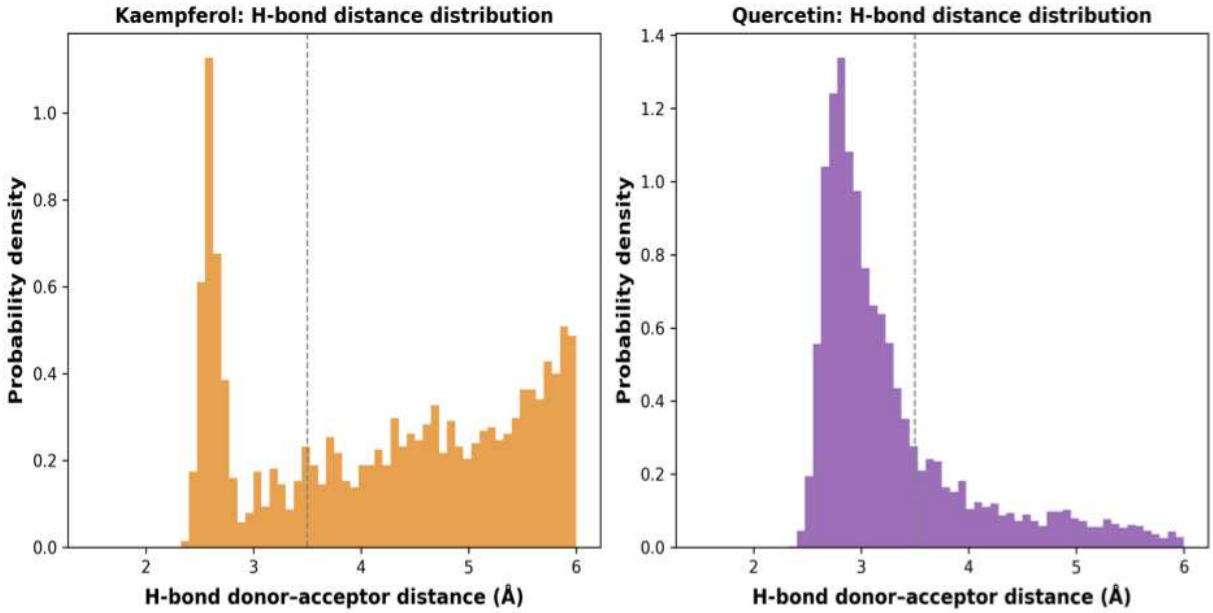


Figure 12. Probability distribution of hydrogen-bond donor–acceptor distances, pooled across all candidate protein–ligand hydrogen bonds and the full 20 ns trajectory, for kaempferol (left) and quercetin (right). The dashed line marks the 3.5 Å bonding cutoff.

Taken together, the time-resolved and occupancy analyses refine the conclusion presented in Section 3.5. Kaempferol loses its only substantial anchor at an early stage and subsequently drifts without a fixed reference point, whereas quercetin retains a stable backbone-mediated anchor throughout the simulation, while the remainder of the molecule becomes mobile. Neither behaviour constitutes the durable, rigid binding expected of a genuine inhibitor, although the underlying mechanisms differ: the engagement of kaempferol is best described as transient, whereas that of quercetin represents a persistent partial anchor with a mobile distal region. This distinction represents a potential target for structure-guided modification. For example, substituents designed to reinforce or extend the backbone anchor of quercetin, or to introduce a second stable point of contact, could plausibly convert a partially anchored pose into one that is durably retained.

3.7 Structural flexibility, compactness, and collective motion

Per-residue root-mean-square fluctuation (RMSF) was calculated for the Cα atoms of both complexes in order to identify locally flexible regions (Figure 13). As the truncated N- and C-termini of the mature LcPPO construct are not held in place by the natural downstream sequence, both chain ends exhibited markedly elevated, non-physiological RMSF values exceeding 10 Å. These values reflect the truncation boundary of the model rather than genuine biological flexibility, and the corresponding residues, comprising the first few N-terminal residues and the region beyond approximately residue 430 approaching the artificial cut point at residue 455, were therefore excluded from further interpretation. Within the structured core (residues 133–430), both complexes displayed a common baseline fluctuation of approximately 0.5–1.5 Å, together with several shared flexible-loop maxima at approximately residues 195–200, 280–285, 320, 350–357 and 383–385. The same loops fluctuated in both trajectories, as would be expected for surface-exposed regions whose motion is largely independent of the bound ligand. The loop spanning residues 195–200 represented a clear exception, as kaempferol induced markedly greater fluctuation in this region (approximately 5.0 Å) than quercetin (approximately 2.8 Å). This region lies adjacent to the Glu331 and Asn332 contacts that constituted the principal, though short-lived, anchor of kaempferol (Section 3.6), suggesting that loss of this anchor destabilised the adjacent loop rather than exerting a purely local effect.

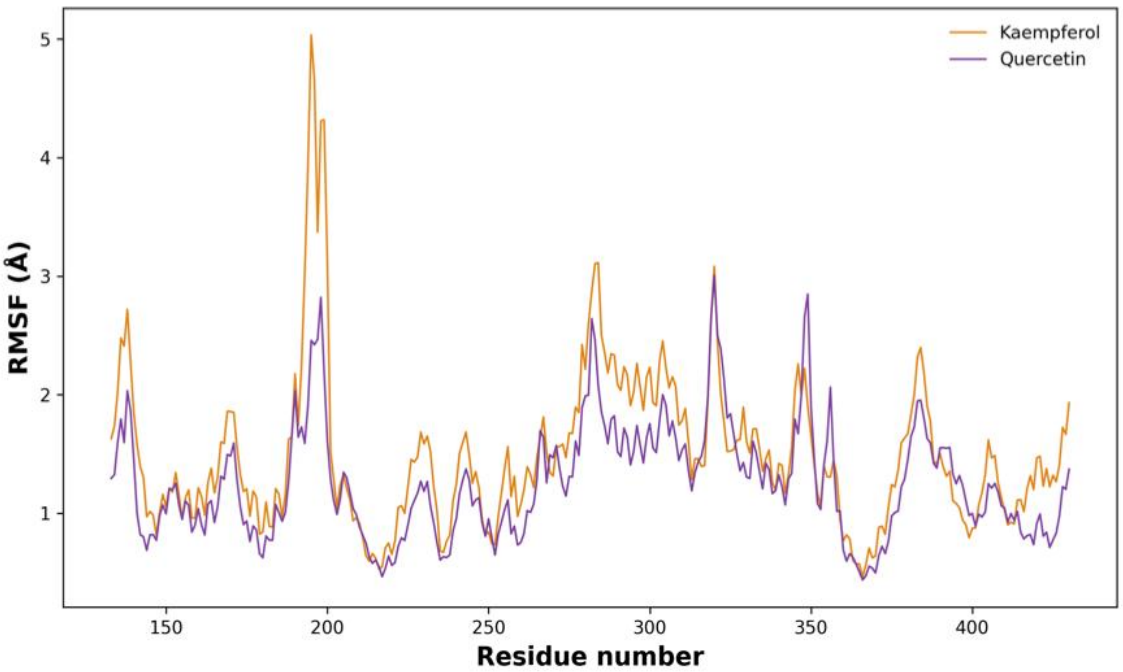


Figure 13. Per-residue RMSF of the Cα atoms of the structured core (residues 133–430) of the kaempferol and quercetin–LcPPO complexes.

The radius of gyration (Rg) of the protein backbone remained within a narrow range for both complexes throughout the simulation, spanning approximately 20.4–21.8 Å for the kaempferol system and approximately 19.8–21.2 Å for the quercetin system, thereby confirming that neither complex unfolded or expanded (Figure 14). The ligand Rg was essentially invariant in both cases, as would be expected for small, rigid flavonol molecules whose intramolecular shape does not vary with position. In contrast, the protein–ligand centre-of-mass (COM) distance provided a clear and independent measure of ligand departure. For kaempferol, the COM distance increased gradually from approximately 12–13 Å to a plateau of approximately 16–17 Å, whereas for quercetin, an abrupt, step-like increase from approximately 13 Å to 19–20 Å was observed at approximately 4–4.5 ns, coinciding with the breakage of its four side-chain hydrogen bonds identified. The convergence of the RMSD, hydrogen-bond and COM-distance analyses upon the same transition at approximately 4–5 ns for quercetin, obtained by three independent methods, provides corroborating evidence that this represents a genuine departure event rather than a statistical artefact.

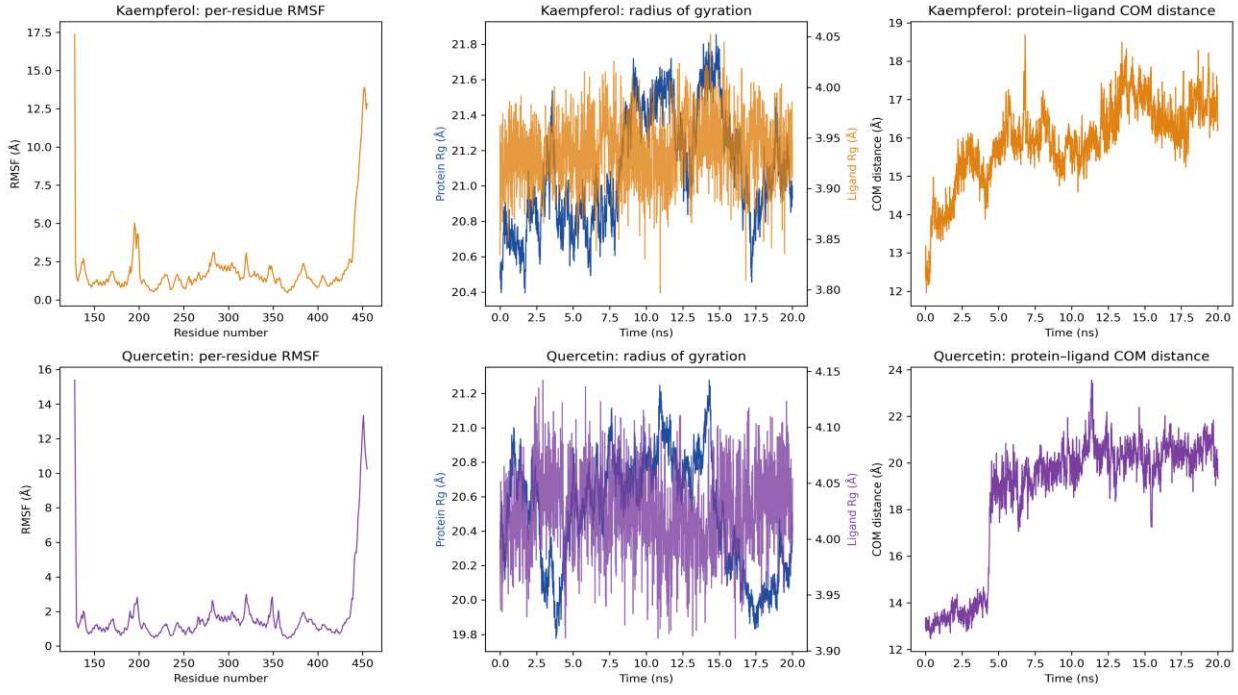


Figure 14. Radius of gyration of the protein backbone and centre-of-mass (COM) distance between protein and ligand over the 20 ns trajectory, for the kaempferol (top) and quercetin (bottom) complexes.

Principal component analysis (PCA) of the backbone Cα coordinates was performed in order to characterise the dominant collective motions of the two complexes (Figure 15). Both trajectories occupied a broad and overlapping region of conformational space along the first two principal components, and no evidence was obtained that the identity of the bound ligand constrained the protein to a distinct conformational basin. The projection along PC1 followed a similar overall course for both complexes, rising over the first approximately 10 ns and falling over the final approximately 5 ns. This behaviour indicates that the dominant backbone motion was associated with the general relaxation of the homology model rather than being driven specifically by the bound flavonol. The observation is consistent with the RMSD analysis presented in Section 3.5, which likewise indicated that the LcPPO backbone had not fully plateaued within 20 ns, and suggests that longer simulations would be required to establish whether the protein settles into a stable conformational basin.

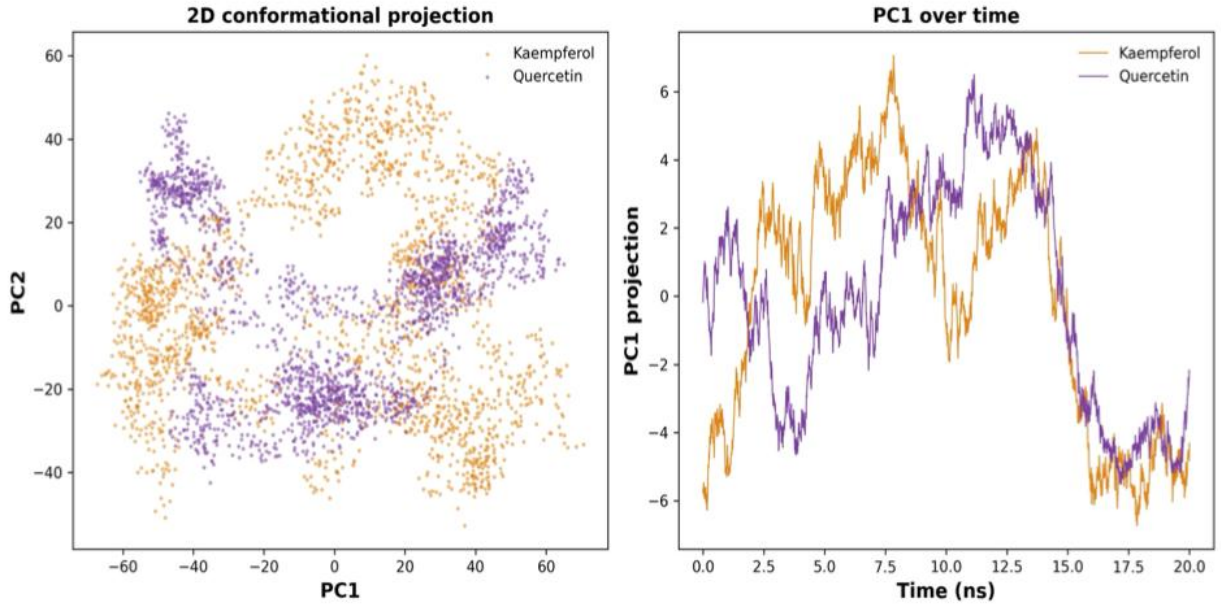


Figure 15. Principal component analysis of backbone Cα motion for the kaempferol (orange) and quercetin (purple) complexes: (left) two-dimensional projection of the trajectory onto the first two

principal components; (right) time evolution of the PC1 projection, showing a similar overall trend for both complexes.

3.8 Mechanistic interpretation and scoring limitation

Several classical PPO inhibitors, including kojic acid (−4.06 kcal/mol) and the reference chelator tropolone (−4.69 kcal/mol), scored below the substrate baseline. This apparent underperformance is expected rather than anomalous. These agents inhibit PPO principally by coordinating the active-site copper ions directly, whereas the empirical Vina scoring function, applied here to a copper-free apo pocket, does not model metal-coordination chemistry. Docking of this type therefore systematically underestimates the affinity of metal-chelating inhibitors, while ranking pocket-binding, substrate-competitive ligands reliably. Accordingly, the conclusions drawn here are confined to the latter class. Among the polyphenols native to litchi, kaempferol and quercetin are predicted to bind the LcPPO active site more strongly than the natural substrate. Metal-chelating inhibitors are more appropriately evaluated by complementary methods that account for copper coordination. A trajectory-averaged binding free energy, for example by MM-GBSA or MM-PBSA including per-residue decomposition, was not pursued in the present study. As both flavonols departed their docked poses during the simulations, a free energy averaged over the full trajectory would combine bound and unbound states and would not yield a well-defined estimate of the binding affinity of the intended pose. Such calculations are meaningful only for genuinely stable complexes and are therefore reserved for the copper-coordinating candidates identified as a priority for future work. More fundamentally, both the docking and the molecular dynamics simulations were performed on a copper-free (apo) receptor, as the binuclear centre cannot be represented by the empirical scoring function or by standard biomolecular force fields without bespoke parameterisation. The present model therefore evaluates non-metal-mediated interactions within the substrate-access channel and does not assess copper-chelation mechanisms. Two consequences follow. First, the affinities reported for the flavonols and for the classical chelators are not directly comparable, since the latter act principally through metal coordination that the model omits; the ranking in Table 1 should accordingly be interpreted within, rather than across, these two mechanistic classes. Second, the absence of predicted contacts between the flavonols and the copper-coordinating histidines reflects the apo-binding mode and does not constitute evidence that these compounds are incapable of copper coordination in the holoenzyme.

3.9 ADMET and drug-likeness of the lead flavonols

Although the molecular dynamics results moderate the binding claims, the two lead flavonols retain considerable value as starting scaffolds owing to their favourable predicted pharmacokinetic and safety profiles, Categorical entries are Yes/No predictions; numeric entries are model outputs in the stated units (Table 3). Both compounds are of low molecular weight (286 and 302 g/mol), moderately lipophilic (consensus Log P values of 1.2 and 0.8) and water-soluble, with high predicted human intestinal absorption (74–77%) and no blood–brain barrier penetration. Both satisfy all major drug-likeness criteria, including Lipinski's rule of five, for which no violations were recorded, with a bioavailability score of 0.55 and favourable synthetic accessibility.

Of particular relevance to a food-related application, neither compound generated major toxicity alerts in the selected in silico prediction models. Both were predicted to be negative for AMES mutagenicity, hepatotoxicity, hERG I and II inhibition, and skin sensitisation, and both exhibited comparable oral rat LD50 values of approximately 2.45–2.47 mol/kg. The only minor alerts identified were a shared, weak inhibition of CYP1A2 and, for quercetin, a single PAINS and Brenk structural alert arising from its catechol moiety. This moiety is the same electron-rich group responsible for the antioxidant and PPO-substrate behaviour of flavonoids, and it constitutes a well-recognised and generally benign feature of dietary polyphenols.

Overall, the ADMET analysis indicates that kaempferol and quercetin possess drug-like physicochemical properties and favourable predicted absorption, and that neither generated major toxicity alerts in the models applied. These predictions support their prioritisation for experimental evaluation, although experimental safety assessment remains necessary before any food application can be inferred. Should such evaluation prove favourable, their anti-browning potential might be realised through chemical modifications conferring durable, copper-coordinating engagement of the PPO active site.

Table 3. Predicted ADMET and drug-likeness properties of the two lead litchi flavonols (SwissADME and pkCSM).

Property	Kaempferol	Quercetin
Physicochemical		
Molecular formula	$C_{15}H_{10}O_6$	$C_{15}H_{10}O_7$

Molecular weight (g/mol)	286.24	302.24
Consensus Log P	1.20	0.79
TPSA (Å²)	111.13	131.36
H-bond donors / acceptors	4 / 6	5 / 7
Absorption and distribution		
Intestinal absorption (% absorbed)	74.29	77.21
Water solubility (log mol/L)	−3.04	−2.93
BBB permeant	No	No
Metabolism		
CYP1A2 inhibitor	Yes	Yes
CYP2C9 / 2C19 / 2D6 / 3A4 inhibitor	No	No
Toxicity		
AMES mutagenicity	No	No
Hepatotoxicity	No	No
hERG I / II inhibitor	No / No	No / No
Skin sensitisation	No	No
Oral rat acute toxicity, LD50 (mol/kg)	2.449	2.471
Max. tolerated dose (log mg/kg/day)	0.531	0.499
Drug-likeness		
Lipinski violations	0	0
Bioavailability score	0.55	0.55
PAINS / Brenk alerts	0 / 0	1 / 1
Synthetic accessibility (1–10)	3.14	3.23

4. Conclusion

A homology model of mature litchi polyphenol oxidase was constructed, its binuclear copper centre reconstituted, and the model validated by re-docking the natural substrate, (−)-epicatechin, which adopted a catalytically plausible orientation. This model enabled the first structure-based screening of candidate anti-browning agents against litchi PPO. Among fourteen compounds screened, kaempferol (−6.89 kcal/mol) and quercetin (−6.58 kcal/mol) obtained the most favourable docking scores, exceeding that of the natural substrate, and both were predicted to

occupy the substrate-access channel. Classical metal-chelating inhibitors scored comparatively weakly, reflecting the inability of the empirical scoring function to represent copper coordination; affinities for the two mechanistic classes are therefore not directly comparable. Independent 20 ns molecular dynamics simulations showed the enzyme to remain structurally stable, whereas neither flavonol persistently maintained its docked pose, although both remained protein-associated throughout. As the backbone had not fully equilibrated and a single trajectory was generated per ligand, these findings characterise early trajectory behaviour rather than converged binding stability. ADMET profiling indicated drug-like properties and no major toxicity alerts, though experimental safety assessment remains necessary. Two boundaries apply. Both docking and simulation used a copper-free receptor, so the work evaluates channel interactions and cannot assess copper-chelation mechanisms. All results are computational predictions; the compounds are candidates for experimental evaluation rather than established inhibitors. Future work should encompass replicate simulations of extended duration, simulations incorporating a parameterised copper centre, and in vitro inhibition assays with browning trials to determine whether these predicted interactions translate into measurable activity.

Acknowledgements

The authors would like to express their sincere gratitude to the Indian Institute of Technology Kharagpur for providing the necessary institutional support and research facilities.

Funding sources

This research did not receive any specific grant from funding agencies in the public, commercial, or not-for-profit sectors.

Authors' contributions

Sakshi Sinha: Conceptualisation; Investigation; Formal analysis; Visualisation; Validation; Writing- original draft; Writing-review & editing. **Rishikesh Ratan:** Investigation, Formal analysis; Visualisation; Validation; Writing- original draft; Writing-review & editing. **Data availability**

The data and code will be made available by the corresponding author upon reasonable request.

References

Alahdal MA, Alahdal H, Binothman N, Aljadani M, Helmi N, Al-Ghamdi MA, et al. Heptapharmacological activity of Quercetin-3-O-phosphate against lung cancer pathways. PLoS One. Public Library of Science San Francisco, CA USA; 2026;21(7):e0349042.

Bhushan B, Pal A, Narwal R, Meena VS, Sharma PC, Singh J. Combinatorial approaches for controlling pericarp browning in Litchi (Litchi chinensis) fruit. Journal of Food Science and Technology. Springer; 2015;52(9):5418–26.

Bolton EE, Chen J, Kim S, Han L, He S, Shi W, et al. PubChem3D: a new resource for scientists. Journal of cheminformatics. Springer; 2011;3(1):32.

Bordoli L, Kiefer F, Arnold K, Benkert P, Battey J, Schwede T. Protein structure homology modeling using SWISS-MODEL workspace. Nature protocols. Nature Publishing Group; 2009;4(1):1–13.

Burendei B, Kaplan JP, Orellana GM, Liman ER, Forli S, Ward AB. Structure-guided discovery of Otopetrin 1 inhibitors reveals druggable binding sites at the intrasubunit interface. Nature Communications. Nature Publishing Group UK London; 2025;16(1):9362.

Castillo-Olvera G, Sandoval-Cortes J, Ascacio-Valdes JA, Wong-Paz JE, Álvarez-Pérez OB, FloresLópez ML, et al. Litchi chinensis: Nutritional, functional, and nutraceutical properties. Food Production, Processing and Nutrition. Springer; 2025;7(1):3.

Daina A, Michielin O, Zoete V. SwissADME: a free web tool to evaluate pharmacokinetics, drug-likeness and medicinal chemistry friendliness of small molecules. Scientific reports. Nature Publishing Group UK London; 2017;7(1):42717.

Deshi V, Homa F, Ghatak A, Aftab M, Mir H, Ozturk B, et al. Exogenous methyl jasmonate modulates antioxidant activities and delays pericarp browning in litchi. Physiology and Molecular Biology of Plants. Springer; 2022;28(8):1561–9.

Di Trani JM, Gheorghita AA, Turner M, Brzezinski P, Ädelroth P, Vahidi S, et al. Structure of the bc 1–cbb 3 respiratory supercomplex from Pseudomonas aeruginosa. Proceedings of the National Academy of Sciences. National Academy of Sciences; 2023;120(40):e2307093120.

Duong VT. Investigation of protein sequence-structure dynamics using bioinformatics, molecular dynamics and machine learning. University of California, Irvine; 2020.

Ehrt C, Schulze T, Graef J, Diedrich K, Pletzer-Zelgert J, Rarey M. Proteins Plus: a publicly available resource for protein structure mining. Nucleic acids research. Oxford University Press; 2025;53(W1):W478–84.

Gunasekaran S, Purushothaman A, Anju K. In Silico Assessment of Cannabidiol From Cannabis sativa as an Antiviral Agent Against Key Shrimp Pathogens in Aquaculture. Journal of Fish Diseases. Wiley Online Library; 2026;49(1):e70015.

Hu Z, Liu Y, Huang Y, Yu P. Advances in the directed evolution of computer-aided enzymes. Current Topics in Medicinal Chemistry. Bentham Science Publishers; 2026;26(2):180–97.

Huang CC, Paull RE, Wang T. Litchi postharvest physiology and handling. Crop Science. Wiley Online Library; 2024;64(4):2014–63.

Jiang Y, Duan X, Joyce D, Zhang Z, Li J. Advances in understanding of enzymatic browning in harvested litchi fruit. Food Chemistry. Elsevier; 2004;88(3):443–6.

Kumar S, Sharma S, Katiyar V. Intelligent & edible biopolymer-based packaging technologies for postharvest shelf-life enhancement of litchi (Litchi chinensis) fruit: a comprehensive review. Sustainable Food Technology. The Royal Society of Chemistry; 2026;4(2):1262–89.

Liang M, He Z, Xiao S, Meng X. Unraveling the Mechanisms and Technologies to Combat Postharvest Deterioration in Litchi: A Comprehensive Review. Journal of Agriculture and Food Research. Elsevier; 2026;102860.

McGibbon RT, Beauchamp KA, Harrigan MP, Klein C, Swails JM, Hernández CX, et al. MDTraj: a modern open library for the analysis of molecular dynamics trajectories. Biophysical journal. Elsevier; 2015;109(8):1528–32.

Mohamed Z. Molecular Dynamics Simulations for Biological Systems: A Review of Theory, Tools, and Protocols Using GROMACS, NAMD, and OpenMM. North Dakota State University; 2025;

Nacif SR, Paoli AAS, Salomão LCC. Morphological and anatomical development of the litchi fruit (Litchi chinensis Sonn. cv. Brewster). Fruits. 2001 July;56(4):225–33.

Noriega HA, Akala EO, Wang XS. Multiscale Computational Studies of PEG Chain Length Effects on HER2 mAb Fc Structure and Binding Energetics. ACS omega. 2025;10(49):60688.

Pollard AT. Seeds vs fungi: an enzymatic battle in the soil seedbank. Seed Science Research. Cambridge University Press; 2018;28(3):197–214.

Rufa D. Improving Prediction Accuracy of Small Molecule Binding and Hydration Free Energies. Weill Medical College of Cornell University; 2025;

Sivakumar D, Terry LA, Korsten L. An overview on litchi fruit quality and alternative postharvest treatments to replace sulfur dioxide fumigation. Food Reviews International. Taylor & Francis; 2010;26(2):162–88.

Tripathi A, Suri K, K S, Murugan NA. Assessing the accuracy of binding pose prediction for kinase proteins and 7-azaindole inhibitors: a study with AutoDock4, Vina, DOCK 6, and GNINA 1.0. RSC advances. The Royal Society of Chemistry; 2025;15(55):47051–65.

Wang S, Li F, Wang G, Li H, Li X, Cao X, et al. Polyphenol oxidase gene editing changed the flavonoid composition and browning process of litchi (Litchi chinensis Sonn.) callus. Gene. Elsevier; 2025;936:149130.

Wang Y, Liu Y, Huang Y, Hou S, Zhu X, Teng J. Characterization and Inhibition of Plant Polyphenol Oxidase for Quality Preservation in Post-Harvest Processing. Food Reviews International. Taylor & Francis; 2026;42(6):4635–57.